Applied Catalysis B: Environmental 182 (2016) 414–423

Contents lists available at ScienceDirect

Applied Catalysis B: Environmental

journal homepage: www.elsevier.com/locate/apcatb

Photocatalytic reductive degradation of polybrominated diphenyl ethers on CuO/TiO_2 nanocomposites: A mechanism based on the switching of photocatalytic reduction potential being controlled by the valence state of copper

Ming Lei[a,b], Nan Wang[b], Lihua Zhu[b,**], Qiaoli Zhou[b], Gang Nie[a], Heqing Tang[a,*]

[a] Key Laboratory of Catalysis and Materials Science of the State Ethnic Affairs Commission and Ministry of Education, College of Resources and Environmental Science, South-Central University for Nationalities, Wuhan 430074, PR China
[b] College of Chemistry and Chemical Engineering, Huazhong University of Science and Technology, Wuhan 430074, PR China

ARTICLE INFO

Article history:
Received 20 July 2015
Received in revised form 7 September 2015
Accepted 15 September 2015
Available online 16 September 2015

Keywords:
Photocatalytic reduction
Reduction potential
Copper oxides
Titanium dioxide
Polybrominated diphenyl ether

ABSTRACT

Highly active CuO-modified TiO_2 (Degussa P25) photocatalysts were prepared by an impregnation method. Efficient and rapid degradation of polybrominated diphenyl ethers were achieved on CuO/TiO_2 photocatalysts. Both TiO_2 and CuO/TiO_2 yielded a rapid photocatalytic reduction of decabromodiphenyl (BDE209). However, the photo-reductive degradation of 2,2′,4,4′-tetrabromodiphenyl ether (BDE47) was impossible on TiO_2, but became fast on CuO/TiO_2. Moreover, the photo-reductive degradation of BDE47 on CuO/TiO_2 needed a short induction time period (20 s) to initiate the reduction. A mechanism was proposed for the enhanced photo-reductive degradation of BDE47 on CuO/TiO_2. During the induction time period, the CuO clusters trapped electrons from TiO_2 to form Cu_2O as confirmed by XPS analysis. Further surface photovoltage and phase spectroscopic analysis and flatband potential measurements were conducted for TiO_2, CuO/TiO_2 and Cu_2O/TiO_2. In the new mechanism, a "switching reduction potential by the valence state of copper" concept was proposed. Because of the higher reduction potential of Cu_2O than CuO and TiO_2, the in-situ composition change led to a Fermi level shift to a more reductive energy for injecting electrons to BDE47, resulting in the initiation of the photocatalytic reduction of BDE47 on CuO/TiO_2. The proposed concept was useful to design and regulate photocatalysts for reductively degrading persistent pollutants.

1. Introduction

In recent years, light driven photocatalytic reduction over TiO_2-based semiconductor has received a great deal of attention, because of its various applications including solar photovoltaics [1], generation of hydrogen [2], conversion of CO_2 to fuel [3], synthesis of amines from nitro compounds [4], remediation of toxic inorganic contaminants (e.g., (Cr(VI))) [5] and organohalide pollutants [6]. However, its low quantum efficiency resulted from mainly a rapid charge recombination has greatly restricted the TiO_2-mediated reduction reactions [7]. To overcome this problem, heterostructured TiO_2 photocatalysts have been constructed. For example, hybrids of TiO_2 and carbon nanomaterial (e.g., C60, carbon nanotube (CNT), and graphene) are shown to have greatly promoted the charge separation across their interface [8–10]. Nobel metal nanoparticles (e.g., Au, Ag, and Pt) were intensively used to quickly capture electrons from photoexcited TiO_2 [11–13]. However, the use of noble metals (such as Ag, Au, Pt, Pd) and special carbon materials (such as CNT and graphene) will certainly increase the cost of the photocatlysts. From this viewpoint, it is interesting to develop new heterostructured photocatalysts by using cheaper earth-abundant elements in easily-prepared speciation such as copper oxides [14].

Monoclinic CuO and cubic Cu_2O are the two main lattice structures of *p*-type copper oxides. The appropriate conduction band edges of both CuO and Cu_2O (0.96 and −1.64 V [15,16], respectively) make them suitable candidates for TiO_2 doping to enhance

* Corresponding author. Fax: +86 27 67843323.
** Corresponding author. Fax: +86 27 87543032.
E-mail addresses: lhzhu63@hust.edu.cn (L. Zhu), tangheqing@mail.scuec.edu.cn, hqtang62@aliyun.com (H. Tang).

http://dx.doi.org/10.1016/j.apcatb.2015.09.031
0926-3373/

the hydrogen production or pollutants degradation. Kum et al. reported that the mixture of TiO_2 nanoparticles and CuO nanoparticles exhibited photocatalytic hydrogen production rate of up to 8.23 mmol h^{-1} g^{-1}, being much higher than that achieved by using the TiO_2 nanoparticles mixed with Pt (2.81 mmol g^{-1} h^{-1}), Au (2.06 mmol g^{-1} h^{-1}), and Ag (0.51 mmol g^{-1} h^{-1}) nanoparticles [17]. Kumar et al. synthesized CuO/TiO_2 nanotubes nanocomposites by a wet-impregnation method, which could produce hydrogen gas at a rate of 99,823 μmol h^{-1} g^{-1} in a water–glycerol mixture, being 25 folds faster than TiO_2 nanotubes [18]. In general, the loaded CuO could act as electron trapper to separate photogenerated electrons and holes of TiO_2 due to their matched band structure, leading to the enhancement of photocatalytic efficiency. Moreover, Hou et al. loaded Cu_2O nanoparticles onto a TiO_2 electrode with a highly ordered vertically oriented nanotube array by using photocatalytic reduction, and the highest photoconversion efficiencies observed for the Cu_2O-loaded electrode are 17.2% under UV light, being higher than that (13.31%) of the TiO_2/Ti nanotube arrays [19]. Zhang et al. deposited a Cu_2O microgrid on the surface of a TiO_2 film, and found that the new. configuration showed higher photocatalytic degradation removal (ca. 80%) for decomposing MB than Cu_2O (ca. 10%) and TiO_2 films (ca. 50%) did with an UV irradiation of 180 min [20]. Unlike the CuO/TiO_2 systems, electron injection is expected from the photoexcited Cu_2O nanoparticles into the CB of TiO_2 because the conduction band (CB) of TiO_2 (−0.45 V) [21] lies more positive than that of Cu_2O (−1.64 V). In contrast, Jung et al. observed that Cu^+/Cu^0 component was responsible for photocatalytic H_2 generation over CuO_x/TiO_2, whereas the Cu^{2+} presence in turn appeared to lower the ability of CuO_x/TiO_2 to generate hydrogen as it could compete with the protons for photogenerated electrons [22]. It is worth noting that the CB edge position of CuO is more positive (0.96 V) than normal hydrogen electrode potential, and the photoexcitation-induced electrons in CuO components cannot produce hydrogen from water [23]. Most researchers speculated that the electron transfer from TiO_2 to CuO increased the Fermi energy level of CuO, leading to the CB position of CuO negative than hydrogen electrode potential [24]. However, Kum et al. declared that the upshift of the CuO Fermi energy level led to the increase in the Fermi level of TiO_2 because of inter-particle electron transfer, and they experimentally confirmed the formation of trapped electrons in TiO_2, reflecting that the electrons were transferred from CuO to TiO_2 [17]. The indistinct explanation demonstrates that the mechanism of photocatalytic reduction over CuO_x/TiO_2 and the enhancement of photocatalytic reductive activity by coupling copper oxides nanoparticles with TiO_2 are not clear. A difficulty in investigating the above mechanism may be that CuO can be reduced to Cu_2O, while Cu_2O can be oxidized to CuO during photocatalytic processes.

Since the location of electrons on compositional semiconductors controls its reductive ability, a proper understanding of the interfacial electron transfer can provide valuable information for designing highly efficient photocatalysts. For example, the photogenerated electrons on the conduction band of TiO_2 could rapidly reduce decabromodiphenyl ether (BDE209), but was ineffective in reducing the low brominated congeners, because that the lower brominated congeners have much lower electron affinities. This led to that TiO_2-mediated photocatalytical reduction is an efficient method to treat BDE209, but it suffers from a drawback of the accumulation of lower brominated congeners such as 2,2′,4,4′-tetrabromodiphenyl ethers (BDE47) [6,25]. However, our present work showed that CuO/TiO_2 composites could rapid photocatalytically reduce not only BDE209 bust also BDE47. By utilizing two kinds of typical polybrominated diphenyl ether (PBDEs), i.e., BDE209 and BDE47, as probe molecules, the relationship between reducing ability of CuO/TiO_2 and the valence state of cuprum was investigated.

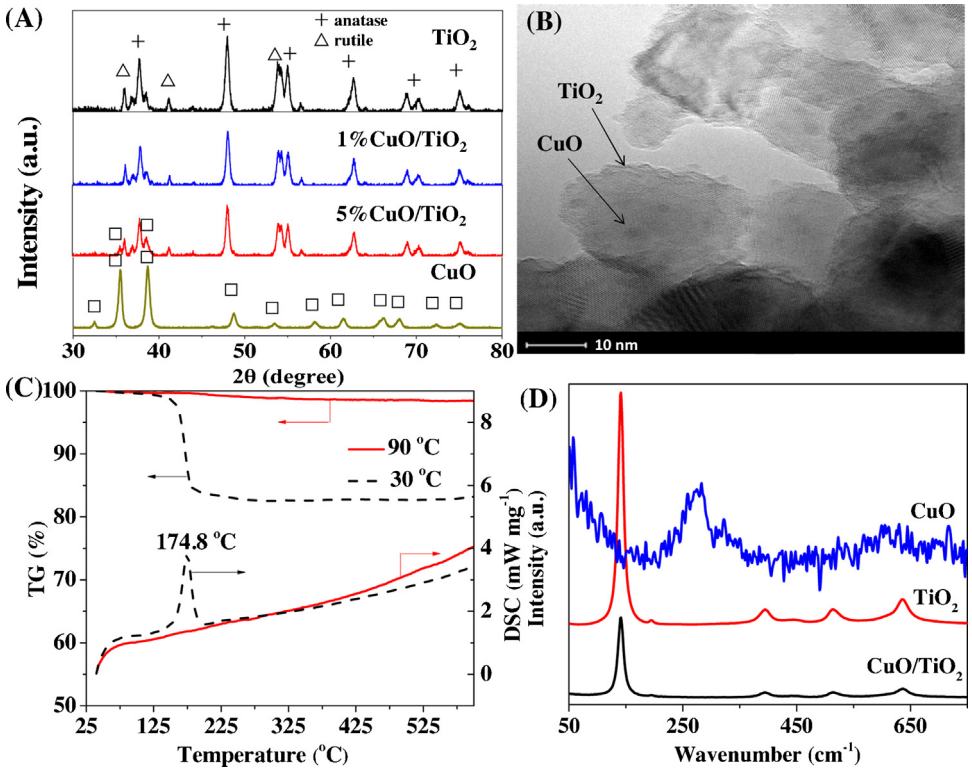

Fig. 1. (A) XRD patterns of pure TiO_2, CuO, and CuO/TiO_2 composites with various Cu contents. (B) TEM images of the 1% CuO/TiO_2 compostite. (C) TGA–DSC curves of Cu species prepared at 30 °C and 90 °C. (D) Raman spectra of pure TiO_2, CuO and 10% CuO/TiO_2 composites. The intensity of CuO was magnified by 1000 times.

2. Experimental

2.1. Chemicals and materials

BDE47 (purity >98.5%) was purchased from J&K Chemical. TiO_2 powders (P25, ca. 80% anatase, 20% rutile; surface area, ca. 50 $m^2 g^{-1}$) was supplied by the Degussa Company (Germany). $CuCl_2{\cdot}2H_2O$ and NaOH (powders) were provided by Sinopharm Chemical Reagent Co., Ltd. All the reagents were analytical grade and used without further purification. Milli-Q water (18.25 MΩ cm) was used for all the experiments.

2.2. Preparation and characterization of CuO/TiO_2 nanocomposites

The CuO/TiO_2 nanocomposites were prepared by an impregnation technique. In a typical process, TiO_2 nanoparticles (1.0 g) were dispersed into distilled water (50 mL), and a certain amount of $CuCl_2$ stock solution was subsequently added to the dispersion. Under stirring, the reaction mixture was incubated in a water bath at 90 °C for 1 h. Then a given amount of NaOH solution was added to the above suspension, which was allowed to react at 90 °C for another 2 h. The final products were sufficiently washed and then dried at 105 °C. The obtained products were referred to as xCuO/TiO_2, where x represented the molar ratio of Cu to Ti, which could be tuned by changing the addition of the $CuCl_2$ stock solution.

The morphology of the CuO/TiO_2 nanocomposites was observed by transmission electron microscopy (TEM) (Tecnai G2 T20, Netherlands) at an accelerating voltage of 200 kV fitted with an EDX accessory. The crystalline structure was characterized by X-ray diffraction (XRD) with monochromatized Cu K_α radiation (Bruker D8 Advance). The accelerating voltage and applied current were 40 kV and 40 mA, respectively. The surface chemical composition of the photocatalysts was investigated by X-ray photoelectron spectroscopy (XPS) on a VG Multilad 2000 spectrometer (Thermo Electron Corporation) with Al K_α radiation as the exciting source (300 W). A PerkinElmer Instrument Diamond TGA/DTA instrument was used for thermal gravimetric analysis (TGA) and differential thermal analysis (DTA). Raman spectra were measured with a DXR Raman Microscopy equipped with a CCD detector (Thermo Fisher Scientific, USA). The 532 nm line of NIR laser was used as an excitation source. The laser power was 1.0 mW at the sample position and the exposure time was set at 1 s with 30 accumulations. Brunauer–Emmett–Teller (BET) surface area was determined by nitrogen adsorption/desorption at 77 K, using a MICROMETERS ASAP 2000 apparatus. Electrochemical measurements were performed in a three electrode quartz cells with 0.1 M Na_2SO_4 electrolyte solution. The samples were prepared by drop casting the composites (or TiO_2) onto a glassy carbon electrode and drying in vacuum oven at 60 °C. A Pt electrode and a saturated calomel electrode (SCE) were used as the counter and reference electrodes, respectively. Photocurrent measurements were conducted in a three-electrode configuration, where the working electrodes have an active area of ca. 2.25 cm^{-2} and Pt electrode and SCE were used as the counter and reference electrodes. The electrolyte utilized in the photocurrent measurement is 1 mol L^{-1} Na_2SO_4 aqueous solution. The working electrodes were prepared as follows: the as-prepared sample (30 mg) was mixed with 10 mL water, and then the mixture was ground to form the slurry. Next, the slurry was coated onto a precleaned F-doped SnO_2 conducting glass (FTO, Dalian Heptachroma Solar Tech Co., Ltd., China) by the doctor blade technique. The prepared electrodes were dried in an oven at 60 °C. A PLS-SXE300 Xe lamp (Beijing Perfect Light Co., Ltd.) was used as the light source. The electrochemical and photoelectrochemical experiment results were recorded with an electrochemical system (CHI-660A). The surface photovoltage (SPV) and phase spectroscopy measurements were carried out based on a lock-in amplifier as described previously [26]. The measurement system consisted of a source of monochromatic light which was provided by a 500 W xenon lamp and a monochromator (SBP500, Zolix), a lock-in amplifier (SR830, Stanford Research System, Inc.) and a sample chamber. The monochromator and the lock-in amplifier were equipped with a computer. The configuration for SPV measurements was a sandwich-like structure. The system was calibrated by a DSI200 UV-enhanced silicon detector to eliminate a possible phase shift which is not correlated to the SPV response, so that any phase retardation reflects the kinetics of the SPV response.

2.3. Photocatalytic degradation of BDE209 and BDE47

The photocatalytic experiments were performed in a quartz vessel with cover. Typically, TiO_2 or CuO/TiO_2 catalysts (20 mg) were added into a BDE47 solution (100 mL), which was obtained by diluting 0.5 mL BDE47 stock solution (1000 mg L^{-1} in tetrahydrofuran) with methanol–water (v:v = 7:3) mixture solvent. The concentration of BDE209 was the same as BDE47, and the solvent for its degradation was changed to 100% mechanol. After the suspension was ultrasonically mixed for 1 min, it was purged with argon for 30 min and protected under argon atmosphere during the photocatalytic experiment. A PLS-SXE300 Xe lamp (Beijing Perfect Light Co., Ltd.) was used as the light source. The photocatalytic experiment was started by switching on the light, and was carried out under magnetic stirring at 30 °C. During the experiment, about 1.5 mL suspension was sampled at given time intervals, and immediately centrifuged at 14,000 rpm for 10 min to remove solid catalysts. The supernatant was filtered through a 0.22 μm membrane and immediately analyzed by high performance liquid chromatography (Agilent 1260 series, USA) equipped with a diode array detector and an SB-C18 column (4.6 × 150 mm). The mobile phase was 90% acetonitrile and 10% water at 1.0 mL min^{-1}, and the detector wavelength was set at 240 nm. All degradation experiments were conducted in duplicate.

3. Results and discussion

3.1. Characterization of catalysts

The hybrid CuO/TiO_2 nanocomposites were prepared by a simple impregnation method. Fig. 1A compared the XRD patterns of pure TiO_2, CuO, and CuO/TiO_2 composites with various Cu contents, which showed typical diffraction peaks of rutile, anatase and CuO structure in the related samples. When the content of Cu was low (x = 1%), no peaks associated with Cu species were observed in the XRD patterns. However, the nanocomposite with a relatively higher Cu content (x = 5%) yielded clear diffraction peaks of CuO at 35.5° and 38.7°, indicating the existence of CuO in the nanocomposite samples. There were no obvious changes in the intensity and half-height widths of the diffraction peaks of anatase and rutile TiO_2, implying that the impregnation of CuO induced no significant change in phase structure and crystallite size of TiO_2. Moreover, no evident shift in the diffraction peaks of TiO_2 was observed for the CuO/TiO_2 composites, suggesting that the deposited CuO clusters adhered on the surface of TiO_2 particles but not incorporated into the lattice of TiO_2.

Fig. 1B shows TEM images of CuO/TiO_2 composites. It was easily found that the CuO/TiO_2 composites consisted of two types of crystalline particles. The first type of particles had sizes of about 25 nm, which were attributed to TiO_2. The second type of particles were CuO clusters with sizes of ca. 1–2 nm, which were uniformly distributed on the surface of TiO_2 nanoparticles by adhering and were confirmed as CuO nanoparticles by EDX analysis (Fig. S1).

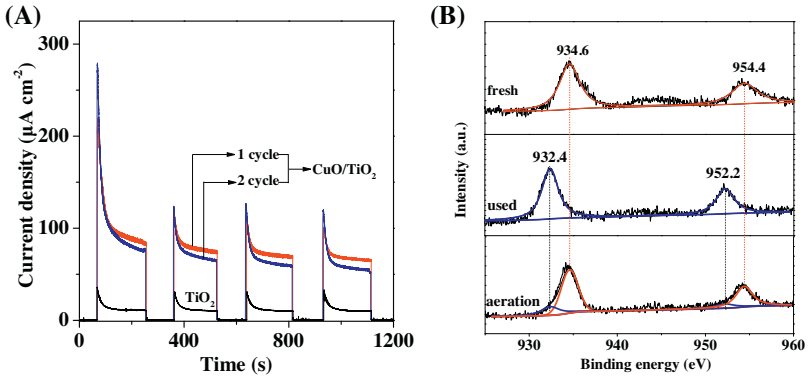

Fig. 2. (A) Transient photocurrent responses of pure TiO_2 and CuO/TiO_2. The fresh CuO/TiO_2 electrode was used for "1 cycle", and the used CuO/TiO_2 electrode after a heat treatment in air was applied for "2 cycle". (B) XPS Cu 2p envelops of (1) fresh CuO/TiO_2, (2) used CuO/TiO_2, and (3) the retreated used-CuO/TiO_2 by aeration for 20 min.

TGA–DSC analysis was carried out to further identify the form of Cu species in the composites. Because the Cu contents in the prepared composites were quite low (less than 5%), the TGA–DSC analysis gave no useful information on the form of Cu species in the composites. We were compelled to prepare the sample with the procedures as the same as that of the composite but without using any TiO_2, and the Ti-free samples were characterized with TGA–DSC in the temperatures ranging from 30 °C to 600 °C. The TGA–DSC curves of the samples prepared at 30 °C and 90 °C were recorded in nitrogen atmosphere as shown in Fig. 1C. When the Ti-free sample was prepared at 90 °C, no obvious mass loss was observed in the TG curve, and no DSC peak was observed in the DSC curve. However, when the Ti-free sample was prepared at 30 °C, the TG curve showed a mass loss of about 18% beyond 25 °C, and the mass-losing step corresponded to an obvious endothermic DSC peak at 174.8 °C, which is attributed to the decomposition of $Cu(OH)_2$ [27]. By calculation, the removal of H_2O from $Cu(OH)_2$ will cause a mass loss of about 18% from the total mass of $Cu(OH)_2$. The above analysis indicates that the Cu species obtained at a low deposition temperature are $Cu(OH)_2$, but that obtained at a high

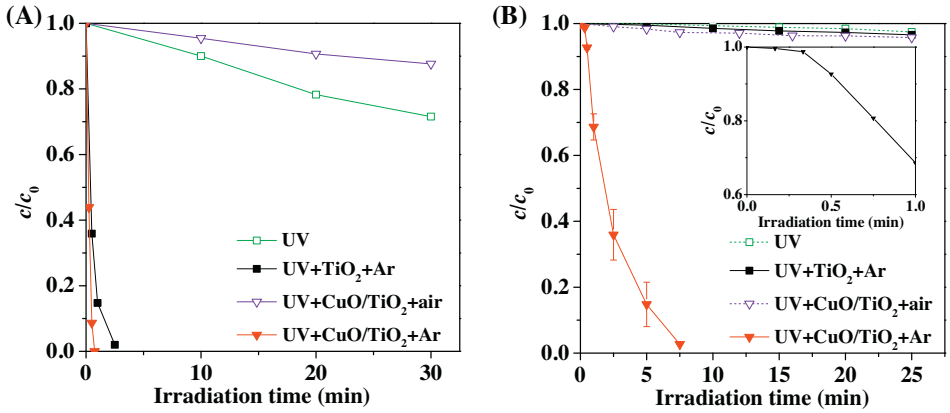

Fig. 3. Photocatalytic degradation kinetics of (A) BDE209 in methanol and (B) BDE47 in a methanol–water (7:3) mixture. Basic reaction conditions were as follows: initial BDE47 (BDE209) concentration, 5 mg L^{-1}; catalyst load, 0.2 mg L^{-1}; gas bubbling: Ar, air or no bubbling. The inset in (B) showed the photocatalytic degradation of BDE47 on CuO/TiO_2 with Ar bubbling for the first minute.

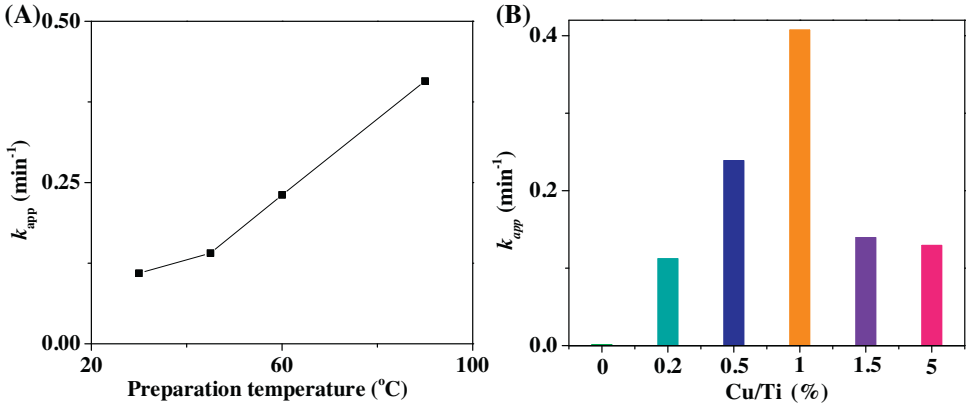

Fig. 4. Effects of (A) preparation temperature and (B) copper content on the apparent rate constant (k_{app}) of BDE47 photocatalytic degradation.

deposition temperature is CuO. In the present work, the CuO/TiO_2 composites were prepared at 90 °C, and hence the involved Cu species in the composite photocatalysts should be substantially CuO but not $Cu(OH)_2$.

Moreover, the chemical composition could also be deduced by Raman spectroscopy. Fig. 1D presented the Raman spectra of TiO_2, CuO and CuO/TiO_2. The anatase phase showed major Raman bands at 144, 197, 399, 515, 519 (superimposed with the 515 cm^{-1} band), and 639 cm^{-1}. These bands can be attributed to the six Raman-active modes of anatase phase with the symmetries of E_g, E_g, B_{1g}, A_{1g} and E_g, respectively. The typical Raman bands due to rutile phase appeared at 143 (superimposed with the 144 cm^{-1} band of anatase phase), which can be ascribed to the B_{1g}, two-phonon scattering, E_g and A_{1g} modes of rutile phase [28]. However, there was no obvious change occurred on the Raman spectra after imported Cu-containing species to TiO_2 in spite of increasing the Cu/Ti ratio to 10%. Thus, we prepared the sample with the procedures as the same as that of the composite but without using any TiO_2, and the Ti-free samples were characterized with Raman spectra. Three Raman-active modes ($A_g + 2B_g$) were observed. We could assign the peak at 282 cm^{-1} to the Ag mode and the peak at 326 and 615 cm^{-1} to the B_g modes of CuO [29]. This result further confirmed that the imported Cu species in the composites were CuO nanoparticles.

3.2. Transient photocurrent response of CuO/TiO_2

The efficient charge separation of photocatalysts is an essential requisite for the photocatalytic activity of CuO/TiO_2. The transient photocurrent response is commonly used to evaluate the efficiency of charge separation. Herein, we conducted the transient photocurrent measurements for photoelectrodes consisting of pure TiO_2 and 1% CuO/TiO_2 nanocomposites. Fig. 2A shows the photocurrent–time (i–t) curves for the aforementioned two samples with several on–off cycles of intermittent irradiation. It was observed that an anodic photocurrent spike occurred at the initial time of irradiation, and subsequently decays quickly until a constant current was reached. Upon switching off the light, the photocurrent disappeared immediately. Under UV irradiation, the photogenerated holes were trapped or captured by reduced species in the electrolyte and the photo-generated electrons within the photoelectrode were transported to the back contact across the samples to lead to the separation of electron-hole pairs at the space charge region and the form of anodic spike photocurrent, and a decay of the anodic photocurrent was generally regarded as the indication of the recombination of photogenerated charges. After the equilibration of competitive separation and recombination of electron-hole pairs, the photocurrent reached a constant value. Thus, it is suggested that the photocurrent is mainly determined by the efficiency of the separation of photo-generated electron-hole pairs within the photoelectrode [30]. Compared with TiO_2, the CuO/TiO_2 sample showed a greater photocurrent, indicating that a more efficient separation of photogenerated electron–hole pairs was achieved in the CuO/TiO_2 composites. It worth noting that unlike TiO_2 which showed stable photocurrent profile, the CuO/TiO_2 sample generated an initial spike current of 279 μA cm^{-2}, but experienced an obvious decreasing in the another on-off illumination cycle. After the cycle, CuO/TiO_2 sample exhibited a good stability performance upon repeating the on–off illumination cycles. This indicates a change in the surface composition of CuO/TiO_2 electrode. Due to the lower potential of the CB energy level, CuO is favorably reduced to Cu_2O or Cu^0 by capturing the photogenerated electrons from the conduction band of TiO_2, resulting in that more photogenerated holes are trapped by reduced species rather than recombined with photogenerated electrons.

XPS profiles provided information on the oxidation state of the elements on the surface of the photocatalyst before and after the UV irradiation. As shown in Fig. 2B, the fresh CuO/TiO_2 sample exhibited Cu 2p3/2 and Cu 2p1/2 peaks at 934.6 and 954.4 eV, respectively, as well as a satellite peak at 944 eV, being indicative of the paramagnetic chemical state of Cu^{2+}. However, the fresh sample showed rather small satellite intensity, which was possibly assigned to two main reasons: the lower amount of copper [31] and the coordination state of Cu^{2+} (the shake-up satellite intensity is stronger for octahedrally coordinated than for tetrahedrally coordinated cupric ion) [32]. After the UV irradiation, the peaks of Cu 2p3/2 and Cu 2p1/2 moved to 932.4 and 952.2 eV, respectively, being assigned to Cu^+ [33]. These revealed that most of surface Cu^{2+} was reduced to Cu^+ upon the UV irradiation. When the Cu_2O/TiO_2 sample was heated in air, it was expected that Cu_2O will be oxidized to CuO. After heating Cu_2O/TiO_2 at 60 °C for 20 min, the observed dominant binding energy (934.6 and 954.4 eV) suggested that the oxidation state of copper on the TiO_2 surface corresponds to Cu^{2+}. This implies a heat treatment led to that most of Cu^+ was re-converted to Cu^{2+} via the oxygen reduction under aerobic conditions, which was in agreement with most of previous reports [34,35]. Accordingly, the used CuO/TiO_2 electrode after a heat treatment showed similar transient photocurrent responses to that observed on the fresh electrode upon beginning another series of on–off illumination cycles (Fig. 2A).

3.3. Photocatalytic reductive activity of CuO/TiO_2

The photocatalytic degradation of BDE209 and BDE47 was used to assess the reductive ability of CuO/TiO_2 (Fig. 3). In control experiments, no matter with the gas bubbling conditions, the direct UV-photolysis and the dark adsorption led to little removal of

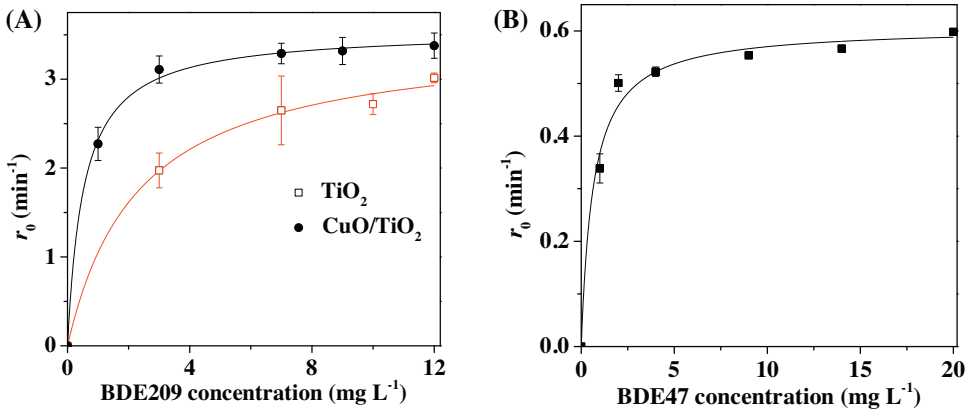

Fig. 5. Pollutant concentration dependence of the degradation rate r_0 of (A) BDE209 and (B) BDE47 over TiO_2 or CuO/TiO_2.

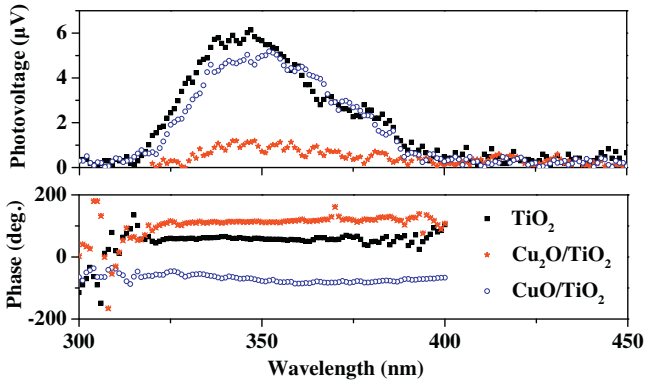

Fig. 6. SPV spectra and corresponding phase spectra of TiO_2, CuO/TiO_2 and Cu_2O/TiO_2.

either of the two PBDEs after 25 min of reaction. Similarly, no degradation of PBDEs was observed on both UV-irradiated TiO_2 and CuO/TiO_2 with the bubbling of air. In UV-irradiation anoxic TiO_2 suspensions, although BDE209 undergoes efficient degradation, the photocatalytic reaction for BDE47 was not detected. However, the degradation of these PBDEs was much more rapid on CuO/TiO_2 in the UV-irradiation anoxic atmosphere, leading to that a degradation removal of almost 100% within 0.75 min and 7.5 min for BDE209, BDE47, respectively. Unlike air bubbling, the Ar bubbling created a reductive atmosphere. Therefore, the rapid degradation of PBDEs was attributed to the photocatalytic reduction mediated by TiO_2 or CuO/TiO_2. The degradation kinetics could be fitted by a pseudo-first-order process, which was expressed as $\ln(c/c_0) = -k_{app}t$,where t is reaction time, k_{app} is the apparent rate constant, and c_0 and c_t are pollutant concentrations at time of $t = 0$ and $t = t$, respectively. The k_{app} values of the photocatalytic reduction of BDE209 and BDE47 (5 mg L^{-1}) on TiO_2 were evaluated as 1.99 and 0 min^{-1}, respectively, but these corresponding values were greatly increased up to 3.19 and 0.41 min^{-1} on CuO/TiO_2, respectively. Here it must be emphasized once more that the photocatalytic reduction of BDE47 was impossible on TiO_2 but became fairly fast on CuO/TiO_2.

The synthesis conditions of CuO/TiO_2 significantly influenced on its photocatalytic activity toward the photocatalytic reduction of PBDEs. Here, a more recalcitrant BDE47 was chosen as a model compound. Fig. 4A illustrated the effect of preparation temperature on the rate constant of photocatalytic degradation of BDE47 over CuO/TiO_2. As the preparation temperature was increased from 30 to 90 °C, the value of k_{app} was almost linearly increased from 0.11 to 0.41 min^{-1}. As discussed in section 3.1 for the TGA–DSC characterization of Cu species in the catalysts, the preparation at 30 °C produced $Cu(OH)_2$, whereas the preparation at 90 °C yielded CuO. It is rational that the product was a mixture of $Cu(OH)_2$ and CuO when the synthesis was carried out at temperatures between 30 and 90 °C. The linear increase of the k_{app} value with increasing the preparation temperature suggests that the photocatalytic activity of CuO/TiO_2 toward the photocatalytic degradation of BDE47 is closely related to the CuO component in the composite photocatalyst. When the photocatalysts prepared at 30 °C are further calcined at 200 °C for 2 h, the $Cu(OH)_2$ coating will be converted to CuO coating. The resulting photocatalysts exhibits much enhanced activity, leading to increasing k_{app} up to 0.40 min^{-1} (almost the same as that obtained from the composite prepared at 90 °C). These phenomenon suggests copper oxide is a more active component than $Cu(OH)_2$. However, a post heat-treatment of CuO/TiO_2 at 200 °C for 2 h, and its photocatalytic activity does not enhance, implying that 90 °C may be enough to prepare CuO/TiO_2 (Fig. S2). Therefore, the synthesis temperature was optimized at 90 °C in the present work.

The content of CuO in the CuO/TiO_2 composite is certainly equivalent to its Cu content, which is easily tuned by changing the addition amount of $CuCl_2$ solution in the preparation. As shown in Fig. 4B, pure TiO_2 showed a small k_{app} value toward the degradation of BDE47 because of the rapid recombination between conduction band (CB) electrons and valence band (VB) holes. With increasing

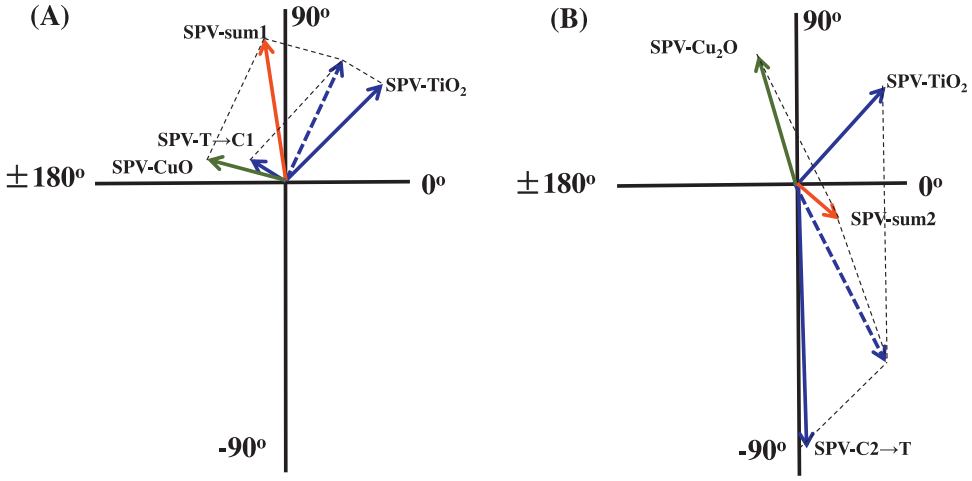

Fig. 7. Vector diagrams of the interaction of three SPV processes arising from the photogenerated charge carriers of (A) CuO/TiO_2 and (B) Cu_2O/TiO_2, in which SPV-TiO_2, SPV-CuO and SPV-Cu_2O are attributed to the SPV processes of TiO_2, CuO and Cu_2O, respectively, while SPV-T → C1, SPV-C2 → T denotes as the SPV processes of TiO_2 that are caused by the interface electric field between CuO and TiO_2, TiO_2 and Cu_2O.

the nominal content of Cu from 0 to 1% (the molar ratio of Cu to Ti), the apparent rate constant of BDE47 degradation was increased from <0.002 min^{-1} to 0.41 min^{-1}. A further increase in Cu content led to a decrease of the photocatalytic activity of the composites. The decrease in the photocatalytic activity of the composited at over-high Cu content ($x > 1\%$) may be partly attributed to (1) shielding the incident light and thus preventing the light adsorption and the generation of photogenerated electrons and holes in TiO_2, (2) shielding the surface active sites of TiO_2 from contacting sacrificial reagents (such as CH_3OH) for the oxidation process, and (3) creating unfavorable charge recombination centers. Therefore, the composition of the CuO/TiO_2 composite photocatalysts was optimized at a Cu content of 1%, which gave the photocatalyst 1% CuO/TiO_2.

3.4. Langmuir–Hinshelwood kinetics of photocatalytic reduction on CuO/TiO_2

Since the photogenerated electron induced reduction reaction occurred on the surface of photocatalysts, the Langmuir–Hinshelwood kinetic model as a qualitative model to describe the solid–liquid heterogeneous reactions, were applied to describe the degradation of PBDEs over photocatalysts [36]. Accordingly, the degradation rate of PBDEs on the surface of photocatalyst will follow Eq. (1)

$$r_0 = \frac{k_r K_a c_0}{1 + K_a c_0} \quad (1)$$

where, r_0 is the initial degradation rate, k_r is the degradation rate constant, and K_a is the apparent adsorption constant, c_0 is the initial concentration of the target pollutant, respectively. The effect of the initial concentration of PBDEs on their degradation rate mediated by TiO_2 and CuO/TiO_2 was shown in Fig. 5. Clearly, r_0 strongly depended on c_0 at low concentration levels, and such dependency relationship becomes progressively weaker at higher pollutant concentrations in all the tested systems. Finally, no further increase in the rate of degradation was obtained with further increasing c_0, inasmuch as saturation coverage (above 5 mg L^{-1}) of the surface active sites on TiO_2 and CuO/TiO_2 was achieved. Moreover, the relationships between c_0 and r_0 are well fitted with Eq. (1), and the resulting K_a value of BDE209 on TiO_2 was 0.43 L mg^{-1}, while the corresponding K_a values of BDE209 and BDE47 over CuO/TiO_2 were 1.88 L mg^{-1} and 1.53 L mg^{-1}, respectively. An analysis of the data depicted in Fig. 5 yielded K_a (BDE209) = 1.88 L mg^{-1} on CuO/TiO_2, which was 4 times larger than that (0.43 L mg^{-1}) on TiO_2. Compared with TiO_2, the enlarged K_a on CuO/TiO_2 is much higher than the increase in its BET surface area (Fig. S3, 49 m^2 g^{-1} for TiO_2 and 61 m^2 g^{-1} for CuO/TiO_2). These results implied that BDE209 preferred to adsorb onto the CuO surface of CuO/TiO_2. Moreover, the K_a value of BDE47 (1.53 L mg^{-1}) and BDE209 were almost equal to each other on CuO/TiO_2. This suggests that CuO/TiO_2 possesses similar binding affinity towards BDE209 and BDE47. When these findings are combined with the fact that the coating of CuO on TiO_2 improved the charge separation by trapping electrons of TiO_2, it is reasonable to propose that the reduction of PBDEs mainly occurred on the surface of CuO rather than on TiO_2 domains. However, unlike the rapid degradation of BDE209 on CuO/TiO_2 at the early reaction stage (Fig. S4), there was a short induction period (20 s) needed in the photocatalytic degradation of BDE47. This indicated that CuO/TiO_2 and/or BDE47 need to undergo a transformation to form reactive species. It is worth noting that the surface Cu^{2+} was reduced to Cu^+, while neither TiO_2 nor BDE47 were changed during this UV irradiation stage. Thus, the in-situ generated Cu_2O may contribute to the photocatalytic reduction of BDE47 CuO/TiO_2.

3.5. Mechanism of enhanced photocatalytic reduction over CuO/TiO_2

Based on the previous reports, quantum-size confinement played an important role on band structure of nanomaterials [37]. To confirm the effect of particle sizes on conduction band of Cu-containing species, the CuO/TiO_2 composites which had been used for the degradation of BDE47 was characterized by TEM. It was observed that the size of particles adhered to TiO_2 was around 2 nm being similar to the fresh CuO/TiO_2 composites (Fig. S5), which demonstrated that the change of degradation behavior between CuO/TiO_2 and Cu_2O/TiO_2 was not arised from the change of particle size.

The above results confirmed that the photocatalytic reduction of PBDEs occurred selectively on the surface of deposited copper oxides cluster, and the coating of CuO on the TiO_2 surface facilitated the charge separation, thereby enhancing the photocatalytic reduction of PBDEs. If shortening the time interval of sampling, it was found that the BDE209 could be reduced directly by the electrons in CuO despite decreasing the illumination intensity of light source (Fig. S4). Separately, an evident induction period (20 s) was required for a subsequent rapid photocatalytic debromination of BDE47 on CuO/TiO_2 (Fig. 3A). However, a pre-UV illumination of 30 min on the CuO/TiO_2 photocatalysts suspension before adding a certain amount of BDE47 stock solution obviously eliminated the occurrence of the induction period (Fig. S6), which suggests that the CuO/TiO_2 photocatalysts undergo a great change after the pre-illumination for 30 min. To clarify the composition change of the photocatalysts used for the degradation of BDE47, the photocatalysts exposured to an illumination of 20 s were obtained by vacuum filtration and subsequently vacuum desiccation for XPS analysis. The XPS analysis (Fig. S7) demonstrated that only cuprous compounds were detected, which indicated that the BDE47 degradation occurred only if the CuO was reduced to Cu_2O. For comparison, the photocatalysts used for the BDE209 degradation were collected in the same way, and the XPS results proved that only small parts of CuO trapped electrons to form Cu_2O, which illustrated that the generation of Cu_2O/TiO_2 was not essential for the degradation of BDE209. This declared that the electrons trapped in CuO can directly contribute to the reduction of BDE209, but not for the reduction of BDE47. Nevertheless, the added BDE47 rapidly disappeared after the loaded CuO gained the photogenerated to form Cu_2O. A good correlation between the reduction rates and the energy level for the lowest unoccupied molecular orbital (E_{LUMO}) of the PBDEs was usually observed in an earlier study [38]. Considering that BDE47 ($E_{LUMO} = -1.518$ eV) has a much lower electron affinity than BDE209 ($E_{LUMO} = -2.419$ eV), thereby the as-synthesized CuO/TiO_2 may obtain higher reduction potential after it is reduced to Cu_2O/TiO_2, suggesting that the enormous difference of interfacial electron transfer existed between CuO/TiO_2 and Cu_2O/TiO_2

SPV spectra were used to reveal the role of interfacial electron transfer between CuO, Cu_2O and TiO_2. The results (SPV and corresponding phase spectra) are shown in Fig. 6. From the SPV spectrum, all the three kinds of photocatalysts showed an obvious response in the ultraviolet region, which is consistent with the intrinsic band gap adsorption of TiO_2. This is because when TiO_2 is excited, photoinduced holes move to the surface of TiO_2 and the positive charge accumulates at the surface of TiO_2 nanoparticles, leading to a positive SPV response arises. Except that, it can be seen that the intensity of the SPV response of CuO/TiO_2 and Cu_2O/TiO_2 is much weaker than that of pure TiO_2. This may be that the lifetime of electron–hole pairs of CuO and Cu_2O is shorter than TiO_2, resulting in the SPV response decreased. Moreover, it can be seen that the phase angle of TiO_2 is about 60°, which does not change during the whole SPV response region. This is because the direction of the built-in electric field of TiO_2 in the surface space charge

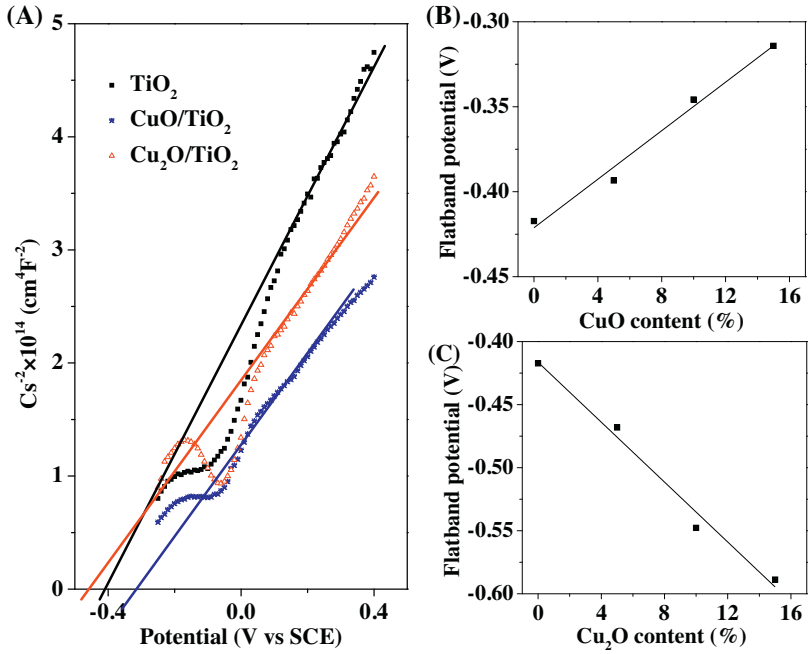

Fig. 8. (A) Mott–Schottky plots of different catalysts film electrodes obtained at a frequency of 10 kHz in an aqueous solution of Na_2SO_4, and flatband potential for TiO_2 with different (B) CuO and (C) Cu_2O content.

region is from the bulk towards the surface, which is expressed as SPV-TiO_2a. After loaded CuO or Cu_2O on TiO_2, the corresponding phase spectrum shifts a lot. As well known, both CuO and Cu_2O are p-type semiconductors due to the presence of copper vacancies [39,40] with a downward surface band bending and the built-in electric field in the surface space charge region orients from the surface towards the bulk, which are marked as SPV-CuO and SPV-Cu_2O and located in 90 and 180°, respectively. Taking CuO/TiO_2 for example, in the 300–400 nm regions, electrons in the valence bands of both TiO_2 and CuO are excited, which are denoted as SPV-TiO_2a and SPV-CuO, respectively. Except that, because of the higher conduction band of TiO_2 (−0.45 V) than CuO (0.96 V), TiO_2 photogenerated electrons can be transferred to the surface of CuO/TiO_2 under the effect of an electric field between the TiO_2 and CuO, which can lead to an SPV response SPV-TiO_2b with phase angle in the range of 90–180°. This indicates that the direction of interfacial electron transfer is from TiO_2 pointing to CuO. These three SPV processes will add according to the rule of vector addition and result in an overall SPV vector SPV-sum1 with phase angle in the range of 90–180° (Fig. 7A). Utilizing similar pathway to analyze phase spectrum of Cu_2O/TiO_2, there is a phase angle of in the range of 0 to −90° appeared besides SPV-TiO_2a and SPV-Cu_2O, which is donated as SPV-TiO_2b′. It is suggested that the direction of the electric field between TiO_2 and Cu_2O is from the former to the latter, which can lead to a positive SPV with electrons transfer away from the surface of the Cu_2O/TiO_2. Overall, the SPV processes of TiO_2 and Cu_2O will be added and lead to a final overall SPV (SPV-sum2) with phase angles in the range of 0 to −90°. The schematic vector diagram is shown in Fig. 7B. Form the SPV phase spectrum analysis, the direction of electron transfer can be summarized as $Cu_2O \rightarrow TiO_2$ and $TiO_2 \rightarrow$ CuO.

To further identify the effect of loaded CuO and Cu_2O on the reduction activity of TiO_2, the flatband potential was determined by electrochemical measurements. From the impedance spectroscopy, Mott–Schottky plots can be obtained according to Eq. (2),

$$C_{sc}^{-2} = \left(\frac{2}{\epsilon\epsilon_0 e N_D S^2}\right)\left(V_B - V_{Fb} - \frac{kT}{e}\right) \quad (2)$$

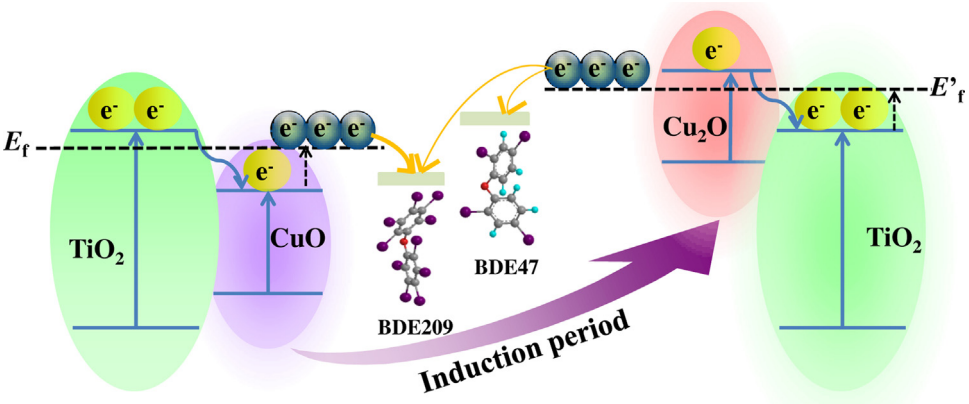

Scheme 1. A mechanism for the photocatalytic reduction of BDE209 and BDE47 on CuO/TiO_2 composites. BDE47 was adsorbed selectively on the CuO clusters in CuO/TiO_2. Upon UV irradiation, the trapped electrons in CuO could inject into BDE209 rapidly but the process is inhibited in thermodynamics for BDE47. Once if the CuO clusters accumulated the electrons to form Cu_2O in situ, the Fermi level would shift to a more negative energy, leading to the fast photocatalytic reduction of BDE47.

where, e is the electron charge, N_D denotes the donor density, ϵ is the dielectric constant of the semiconductor, ϵ_0 is the vacuum permittivity, T is the absolute temperature, k is the Boltzman constant, and S is the surface area of the electrode [41]. The intersection point of the potential and linear potential curves give a flatband potential. The Mott–Scottky plots for pure TiO_2, 5% CuO/TiO_2 and 5% Cu_2O/TiO_2 are shown in Fig. 8A, which give their flatband potentials of approximately −0.42 V, −0.31 V and −0.59 V versus SCE, respectively. Our data for TiO_2 are similar to that reported by Radecka et al. [41]. The flatband potentials of TiO_2 with various CuO or Cu_2O contents were shown in Fig. 8B and C. As shown in Fig. 8B, the flatband potential gradually shifts to positive values with increasing CuO content due to the lower CB position of CuO (0.96 V) than TiO_2 (−0.45 V). Therefore, a fraction of electrons may transfer from TiO_2 to CuO. However, in the case of Cu_2O, the flatband potential moves to negative positions with increasing Cu_2O content (Fig. 8C) because of the higher CB position (−1.64 V) than TiO_2. The results are in agreements with the SPV analysis, further indicating that once if the loaded CuO trapped electrons from TiO_2 to form Cu_2O, the reduction potential of the composites would shift to more negative level.

Based on the discussion above, a conceivable mechanism of PBDEs degradation on CuO/TiO_2 was proposed as Scheme 1. At first, PBDEs were adsorbed selectively on the surface of deposited copper oxides nanoparticles. Upon UV irradiation, TiO_2 would absorb UV light directly to generate holes and electrons, which then migrate to the surface of the particles. As the conduction band of CuO (0.96 V) lies lower than that of TiO_2 (−0.45 V), the presence of CuO nanoparticles on TiO_2 created a thermodynamically feasible pathway to shuttle the electrons photogenerated in TiO_2. Furthermore, because CuO is a p-type semiconductor and TiO_2 is an n-type semiconductor, the electron–hole separations are also driven by the built-in electric fields in the heterojunction, resulting in Fermi level equilibration (E_f). The efficient separation of electrons and holes achieved on CuO/TiO_2, leading to higher reduction rates of BDE209 over CuO/TiO_2 than that over pure TiO_2. However, unlike the rapid degradation of BDE209 on CuO/TiO_2 at the early reaction stage, there was a short induction period (20 s) needed in the photocatalytic degradation of BDE47. During the induction period, the loaded CuO accumulated excess electrons to render the formation of Cu_2O. The CB and VB of Cu_2O lie above those of TiO_2, facilitating the separation of photogenerated holes and electrons. Similarly, there would be an equilibrium Fermi level (E'_f) reached between Cu_2O and TiO_2. Because of the higher flatband potential of Cu_2O/TiO_2 than TiO_2 and CuO/TiO_2, it may exceed the reduction potential of BDE47. After the induction period, the electron transfer from the generated Cu_2O to the adsorbed BDE47 molecules, initiating the rapid photo-reductive degradation of BDE47.

4. Conclusion

The CuO/TiO_2 composites were prepared by a simple impregnation method, and the preparation temperature and Cu content were optimized to 90 °C and 1%, respectively. Rapid photocatalytic reductive degradation of BDE209 could be achieved on both pure TiO_2 and CuO/TiO_2. However, we observed that the photocatalytic reduction of BDE47 was impossible on pure TiO_2 but it was fast on CuO/TiO_2. Moreover, the photo-illumination on CuO/TiO_2 started the photocatalytic reduction of BDE209 on the instant, but there was a short induction time period to initiate the photocatalytic reduction of BDE47, which were closely related to the band structures of the photocatalyst and the LUMO levels of the PBDEs. The present work not only illuminated the important role of CuO nanoparticles on the enhancement of photocatalytic reduction of BDE209, but also explained the criticality of in-situ formed Cu_2O nanoparticles for the photo-reductive degradation of BDE47 as a typical pollutant being much more resistant to reduction. A mechanism was proposed for the peculiarly-enhanced photocatalytic reduction of BDE47 on CuO/TiO_2. According to the new mechanism, the loaded CuO accumulated excess electrons transfer from TiO_2 to form Cu_2O in situ during the induction time period. Because of the more negative reduction potential of Cu_2O than CuO and TiO_2, the in-situ composition change would lead to a Fermi level shift to a more reductive energy for injecting electrons to BDE47 molecules adsorbed on newly-formed Cu_2O/TiO_2, which initiates the rapid photocatalytic reduction of BDE47.

Acknowledgments

The authors acknowledge the financial supports from the National Natural Science Foundation of China (Grants Nos. 21377169, 21177044 and 21107027), and the Research Foundation for Talented Scholar from Huazhong University of Science and Technology (No. 0124013800).

Appendix A. Supplementary data

Supplementary data associated with this article can be found, in the online version, at http://dx.doi.org/10.1016/j.apcatb.2015.09.031.

References

[1] U. Bach, D. Lupo, P. Comte, J.E. Moser, F. Weissörtel, J. Salbeck, H. Spreitzer, M. Grätzel, Nature 395 (1998) 583–585.
[2] Q. Xiang, J. Yu, M. Jaroniec, J. Am. Chem. Soc. 134 (2012) 6575–6578.
[3] J. Yu, J. Low, W. Xiao, P. Zhou, M. Jaroniec, J. Am. Chem. Soc. 136 (2014) 8839–8842.
[4] H. Tada, T. Ishida, A. Takao, S. Ito, Langmuir 20 (2004) 7898–7900.
[5] G. Jiang, Z. Lin, C. Chen, L. Zhu, Q. Chang, N. Wang, W. Wei, H. Tang, Carbon 49 (2011) 2693–2701.
[6] C. Sun, D. Zhao, C. Chen, W. Ma, J. Zhao, Environ. Sci. Technol. 43 (2009) 157–162.
[7] M.R. Hoffmann, S.T. Martin, W. Choi, D.W. Bahnemann, Chem. Rev. 95 (1995) 69–96.
[8] P.V. Kamat, I. Bedja, S. Hotchandani, J. Phys. Chem. 98 (1994) 9137–9142.
[9] Y. Yao, G. Li, S. Ciston, R.M. Lueptow, K.A. Gray, Environ. Sci. Technol. 42 (2008) 4952–4957.
[10] M. Lei, N. Wang, L. Zhu, C. Xie, H. Tang, Chem. Eng. J. 241 (2014) 207–215.
[11] V. Subramanian, E. Wolf, P.V. Kamat, J. Phys. Chem. B 105 (2001) 11439–11446.
[12] A. Takai, P.V. Kamat, ACS Nano 5 (2011) 7369–7376.
[13] N. Zhang, S. Liu, X. Fu, Y. Xu, J. Phys. Chem. C 115 (2011) 9136–9145.
[14] J. Ran, J. Zhang, J. Yu, M. Jaroniec, S. Qiao, Chem. Soc. Rev. 43 (2014) 7787–7812.
[15] Z. Wang, Y. Liu, D.J. Maritin, W. Wang, J. Tang, W. Huang, Phys. Chem. Chem. Phys. 15 (2013) 14956–14960.
[16] L. Zhang, J. Li, Z. Chen, Y. Tang, Y. Yu, Appl. Catal. A: Gen. 299 (2006) 292–297.
[17] J.M. Kum, S.H. Yoo, G. Ali, S.O. Cho, Int. J. Hydrogen Energy 38 (2013) 13541–13546.
[18] D.P. Kumar, M.V. Shankar, M.M. Kumari, Chem. Commun. 49 (2013) 9943–9945.
[19] Y. Hou, X. Li, X. Zou, X. Quan, G. Chen, Environ. Sci. Technol. 43 (2009) 858–863.
[20] J. Zhang, H. Zhu, S. Zheng, F. Pan, T. Wang, ACS Appl. Mater. Interfaces 1 (2009) 2111–2114.
[21] A. Zaban, O.I. Mićić, B.A. Gregg, A.J. Nozik, Langmuir 14 (1998) 3153–3156.
[22] M. Jung, J. Scott, Y.H. Ng, Y. Jiang, R. Amal, Int. J. Hydrogen Energy 39 (2014) 12499–12506.
[23] Z. Jin, X. Zhang, Y. Li, S. Li, G. Lu, Catal. Commun. 8 (2007) 1267–1273.
[24] J. Bandara, C.P.K. Udawatta, C.S.K. Rajapakse, Photochem. Photobiol. Sci. 4 (2005) 857–861.
[25] C. Sun, J. Zhao, H. Ji, W. Ma, C. Chen, Chemosphere 89 (2012) 420–425.
[26] L. Chen, S. Li, Z. Liu, Y. Lu, D. Wang, Y. Lin, T. Xie, Phys. Chem. Chem. Phys. 15 (2013) 14262–14269.
[27] Y. Matsuo, K. Hatase, Y. Sugie, Chem. Mater. 10 (1998) 2266–2269.
[28] J. Zhang, M. Li, Z. Feng, J. Chen, C. Li, J. Phys. Chem. B 110 (2006) 927–935.
[29] W. Yao, S. Yu, Y. Zhou, J. Jiang, Q. Wu, L. Zhang, J. Jiang, J. Phys. Chem. B 109 (2005) 14011–14016.
[30] Q. Xiang, J. Yu, M. Jaroniec, J. Phys. Chem. C 115 (2011) 7355–7363.
[31] M.S.P. Francisco, V.R. Mastelaro, J. Phys. Chem. B 105 (2001) 10515–10522.
[32] S. Contarini, L. Kevan, J. Phys. Chem. 90 (1986) 1630–1632.

[33] K. Lalitha, G. Sadanandam, V.D. Kumari, M. Subrahmanyam, B. Sreedhar, N.Y. Hebalkar, J. Phys. Chem. C 114 (2010) 22181–22189.
[34] H. Yu, H. Irie, K. Hashimoto, J. Am. Chem. Soc. 132 (2010) 6898–6899.
[35] P. Wang, Y. Xia, P. Wu, X. Wang, H. Yu, J. Yu, J. Phys. Chem. C 118 (2014) 8891–8898.
[36] V.K. Sharma, C.R. Burnett, W. Riversa, V.N. Joshi, Langmuir 17 (2001) 4598–4601.
[37] A. Kubacka, M. Fernández-García, G. Colón, Chem. Rev. 112 (2012) 1555–1614.
[38] J. Hu, L. Eriksson, Åke Bergman, E. Jakobsson, E. Kolehmainen, J. Knuutinen, R. Suontamo, X. Wei, Chemosphere 59 (2005) 1043–1057.
[39] C.M. McShane, K. Choi, J. Am. Chem. Soc. 31 (2009) 2561–2569.
[40] A. Kargar, Y. Jing, S.J. Kim, C.T. Riley, X. Pan, D. Wang, ACS Nano 7 (2013) 11112–11120.
[41] M. Radecka, M. Rekas, A. Trenczek-Zajac, K. Zakrzewska, J. Power Sources 181 (2008) 46–55.